



PERGAMON

Available online at www.sciencedirect.com

SCIENCE @ DIRECT®

International Journal of Impact Engineering 30 (2004) 69–86

INTERNATIONAL
JOURNAL OF
**IMPACT
ENGINEERING**

www.elsevier.com/locate/ijimpeng

High-resolution optical study of the impact of carbon-fibre reinforced polymers with different lay-ups

R.I. Hammond*, W.G. Proud, H.T. Goldrein, J.E. Field

Cavendish Laboratory, Madingley Road, Cambridge CB3 0HE, UK

Received 27 February 2002; received in revised form 11 October 2002; accepted 25 March 2003

Abstract

The impact deformation of carbon-fibre reinforced polymer samples with different lay-ups was studied using high-speed optical techniques. The in-plane deformation of the sample was measured using time-resolved fine-grid analysis. The residual velocities of the projectiles were determined using streak photography and hence the energy dissipated during the penetration was obtained. Both microscopic damage and macroscopic damage to the plates were studied. The deformation, energy dissipation and damage all had a strong dependence on the composite lay-up. Unidirectional composites exhibited anisotropic behaviour and were significantly weaker than the other lay-ups. Though this is intuitively reasonable, this paper gives *quantitative* measures of this effect. Composite samples examined using the fine-grid technique exhibited cracking in the rear ply surprisingly early in the impact with wide-reaching delamination of this ply. Comparative measurements are presented for polymethylmethacrylate which deformed more isotropically until fragmentation.

© 2003 Elsevier Science Ltd. All rights reserved.

Keywords: Composite; Impact; Optical technique

1. Introduction

The ballistic performance of lightweight materials is an area of active research [1–3]. The driving force comes from the need to improve the performance of personal protective armour, the toughening of portable equipment and increasing the crashworthiness of vehicles for which significant added weight is undesirable. Fibre reinforced composites are one material group which

*Corresponding author.

E-mail address: rih22@cam.ac.uk (R.I. Hammond).

Table 1
Detailed lay-up of composites used

Series	Comment	Thickness (mm)	Number of plies	Lay-up
A	Quasi-isotropic	2.24	16	$[0^\circ/-45^\circ/45^\circ/90^\circ]_{2s}$
B	Quasi-isotropic	2.53	18	$[0^\circ/60^\circ/-60^\circ]_{3s}$
C	Uni-directional	1.76	12	

Note: $[A/B/C]_{2s}$ corresponds to the lay-up ABCABCCBACBA.

is of great interest given the variety of fibre types, matrix materials and lay-ups possible, resulting in a wide range of shapes, thickness and responses of components [4].

Composite materials are also used extensively in the aircraft industry where impact properties are very important in terms of collision with debris, rain, hail or birds. Given the wide range of possible composites, it is therefore important that the impact response is both understood and predictable.

By incorporation of different components, the mechanical properties of the structure can be tailored to performance requirements. The properties of composites are markedly different to those of the individual components and are determined by the microstructure, specified by the volume fraction and morphology of reinforcement [5], and the properties of the matrix–reinforcement interface. Their impact strength is strongly dependent on the adhesion between the fibre and the matrix, as mechanisms of energy dissipation are yielding within the polymer and delamination [2]. For brittle matrices such as epoxies, mechanisms of energy dissipation such as debonding and fibre pull-out are expected to be suppressed.

In this paper, we report the response to impact of both a unidirectional composite, where the fibres are all parallel to one another, and a quasi-isotropic composite, where layers of fibres are oriented differently between layers. The composite used was a carbon-fibre reinforced polymer (CFRP) fabricated from unidirectional carbon fibre/epoxy prepegs (Batch: Fibredux 924-T800-12K-34%) with a resin content of 34% and a fibre diameter of 6 μm . Samples were 120 mm \times 120 mm; the thickness depended on the number of plies. Table 1 gives the detailed lay-ups used in this research. Generally, the failure strain of carbon fibre is 3–4% at all strain rates [5,6]. In order that comparisons could be made with a more isotropic material, a parallel series of experiments were carried out using polymethylmethacrylate (PMMA).

In many impact studies, investigators have looked at the damage *after* impact and used inference. By the use of high-speed photography operating at microsecond framing intervals, the failure processes can be followed in detail. Additionally, a fine-grid technique has been developed [7–9] which, using high-speed imaging on the timescale of the impact, allows the in-plane deformations, and hence the in-plane strain fields, to be obtained to high precision. This type of information is extremely useful when developing finite element models. The four main results presented here involve: the quantitative analysis of the in-plane deformation of the samples, the quantitative out-of-plane deformation of the target, the kinetic energy loss of the projectile and the damage to the panels all in relation to the lay-up.

2. Experimental procedure

A schematic of the set-up is shown in Fig. 1. The gun reservoir is pressurised with helium and the gun fired by fast-acting valves. The projectile is accelerated down the barrel into the impact chamber. Both chamber and barrel were evacuated to 100 mbar pressure prior to firing. This reduces the amount of air being ejected from the barrel and therefore prevents disturbance of the target prior to impact.

The velocity of the projectile is measured by the projectile cutting two light beams a known distance apart. The error in the system is $\leq 2\%$. The output of the timer was sent to a Hadland Multi-Channel Delay Generator which triggered the flash unit (Bowen Monolight 400), and a High-Speed Image Converter Camera (Ultranac 501). Images were recorded onto Polaroid 667 film and then digitised using a high-resolution flatbed optical scanner. The projectile and debris were decelerated in a catcher chamber (Fig. 1) packed with plywood and foam. The projectile and the target were recovered after each shot.

It was important that sample supports did not obscure the field of view of the camera or strengthen the panel. In practice, the sample was lightly held at the four corners, the bottom two corners were more constrained than the top two, and this was found to affect the final fragment size of the unidirectional samples. With the fibres aligned vertically, the resulting debris pieces were about twice the size than when the fibres were aligned horizontally. Therefore, shots were carried out in both orientations. However, the *initial* response of the panel to the impact was the same in either orientation, as early in the process the in-plane stress waves have not had time to reach and return from the supports, despite the high wave-speed in carbon fibres [10]. Assuming a wave velocity of $10 \text{ mm}/\mu\text{s}$, the time before waves return is $12 \mu\text{s}$. In Fig. 3, for example, waves would not return before frame 12. Additionally, Figs. 4 and 5 show perforation before any detectable flexing of the target.

Steel spheres, 12.7 mm diameter, were fired at an impact velocity of 460 m/s giving an impact kinetic energy of 880 J. All the experiments described here were performed at normal impact. The

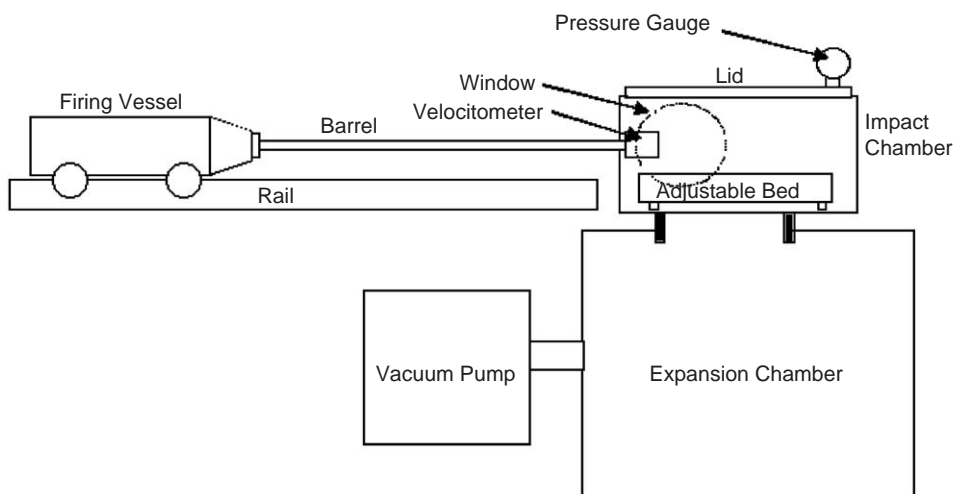


Fig. 1. Schematic diagram of the basic set-up of the gas gun (not to scale).

experiments can be divided into three types; those analysed using the fine-grid technique, those observed using framing photography and those observed using streak photography.

2.1. Fine-grid technique

If a regular array of lines is added to a sample, studying their relative motion will reveal the deformation, allowing the in-plane strain to be calculated. For this research, the rear face of each sample was painted white and grids of pitch 1.5 mm were drawn using a pen held in a computerised milling machine. The lines in the grid were at right angles to one another over the central 75 mm × 75 mm area. This method of grid production was found to be the simplest way to obtain sufficient contrast for high-speed photography [7].

Three squares of the grid, close to, but not in the expected zone of deformation, were filled in to act as fiducial markers. The set-up is shown schematically in Fig. 2. In order to allow sufficient illumination of the rear face of the target, one side of the impact chamber was made from 10 mm thick polycarbonate sheet. Fifteen frames were recorded during each impact and the picture layout is illustrated in Fig. 3. An interframe time of 1 μ s and an exposure time of 0.5 μ s were used. Visual examination of the frames leads to qualitative understanding. For quantitative measurement, these images were digitised and fringe analysis was performed, using a Sun Ultra 1/170 computer, to produce displacement maps [7].

The computational process involves spatially filtering the horizontal and vertical components of the grid, producing x and y phase maps for each frame. Fourier transformation and phase unwrapping were used with one of the fiducial markers defined as a zero reference point. Points of given x and y displacement are tracked between frames by an iterative technique. Hence,

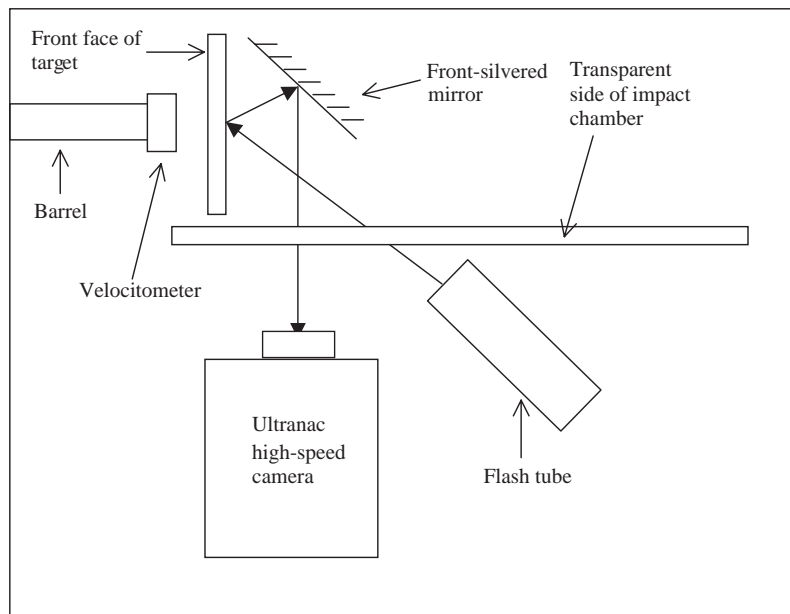


Fig. 2. Schematic diagram of optical layout for fine-grid shots (not to scale).

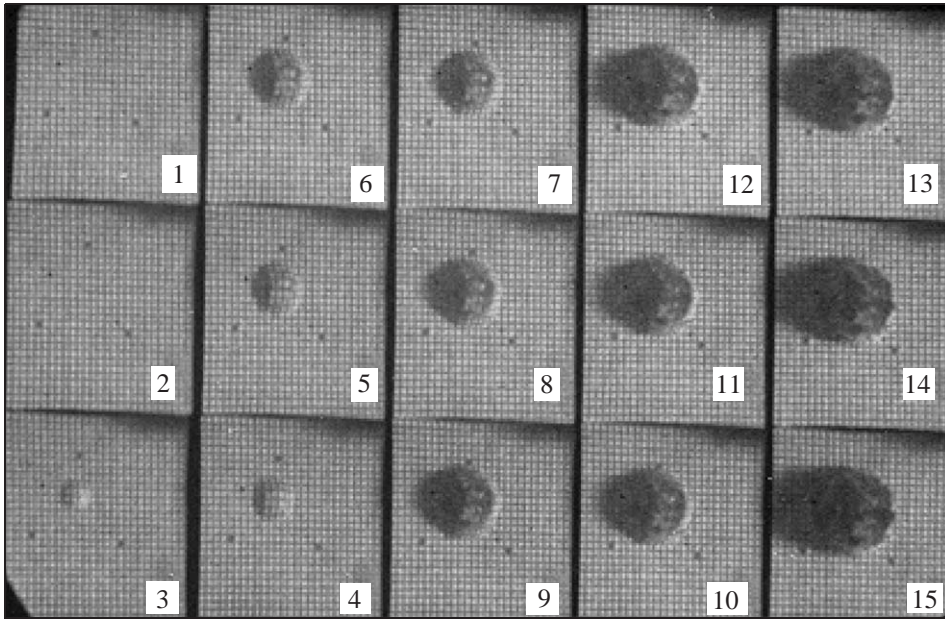


Fig. 3. A 12.69 mm diameter spherical steel projectile impacts a type B composite at 480 m/s. The grid pitch is 1.5 mm. Interframe time $1 \mu\text{s}$, exposure time $0.5 \mu\text{s}$.

displacement maps can be calculated for each frame. For a more detailed description of this process see Goldrein et al. [8].

2.2. Side-view

High-speed images were taken from the side, the firing conditions being identical to those used for the fine-grid technique. Sequences were obtained for each lay-up of composite and also for PMMA.

2.3. Streak photography

In streak photography the event is looked at through a slit. The slit is streaked across the film to give a trace which is essentially a plot of displacement against time along the slit axis. A stationary object in the field of view will appear as a horizontal line, a moving object will appear as a diagonal band, the slope of which is proportional to the velocity of the object. If the streak rate is known, then velocities can be calculated. The axis observed was along the centre line of the barrel. Streak photography results in velocity–time measurements of high accuracy (typically $\pm 1\%$). The residual velocity of the projectile after impact was used to calculate the energy absorbed during the impact. Accurate measurement of the streak rate was required so calibration was performed by monitoring the movement of a projectile with known velocity. The streak rate was found to be $1.21 \pm 0.01 \mu\text{s}/\text{mm}$.

2.4. Microscopy

Material from around the penetration site was potted and subjected to optical microscopy. In sectioning, some damage to the composite was inevitable, therefore, about 2 mm of each sample was ground off before final polishing. Fracture faces were gold sputtered and examined using a JEOL JSM-820 Scanning Electron Microscope (SEM).

3. Results

During impact, clouds of debris were ejected from both the front and rear of the composite (Fig. 4). This cloud probably consists of highly fragmented fibre and matrix components. The side-on records display a bulge on the rear face of the sample that was obscured by the debris cloud after only a small number of frames had been obtained (Fig. 4). However, the presence of a debris cloud may indicate that the rear of the target has “ceased to exist” in the impact zone. Once the fibres have fractured into small enough fragments the matrix around these fragments can no longer act as stress transmitters, while the matrix undergoes shear leading to failure of the panel [11]. During the impact with PMMA, debris was only ejected from the rear of the target (Fig. 5). Considering the nature of fragmentation in each case: the PMMA samples developed a few long continuous cracks which dissipates less fracture surface energy than the composite.

The projectile penetrated all samples during impact. The panel was of a size that it could not respond by flexure on the timescale of the fracture despite the high wave-speed in the fibres [10]. High stresses were therefore generated at the point of impact and led to failure. Deformation of

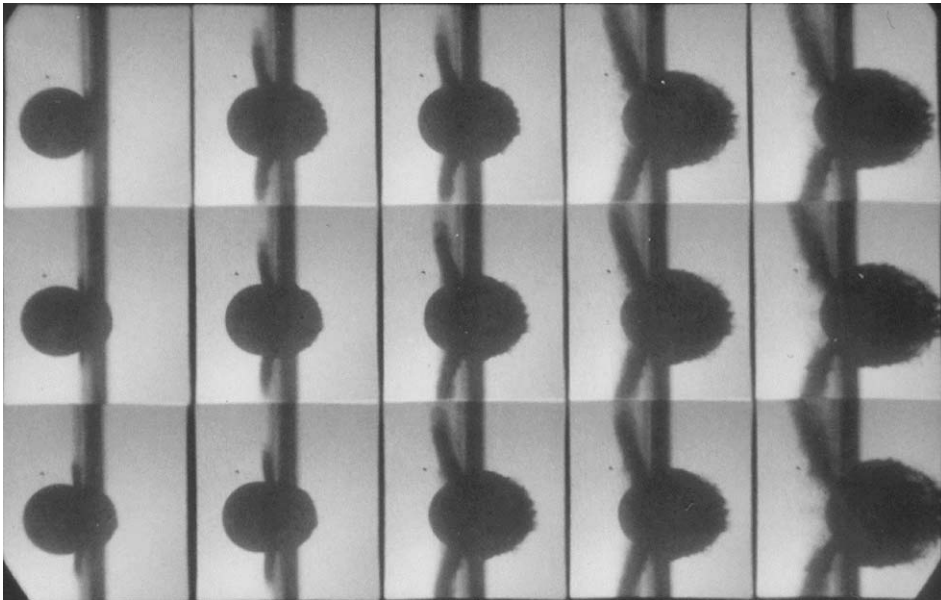


Fig. 4. An example record of 12.69 mm diameter spherical steel projectile impacting type B composite at 460 m/s. Interframe time 1 μ s, exposure time 0.5 μ s.

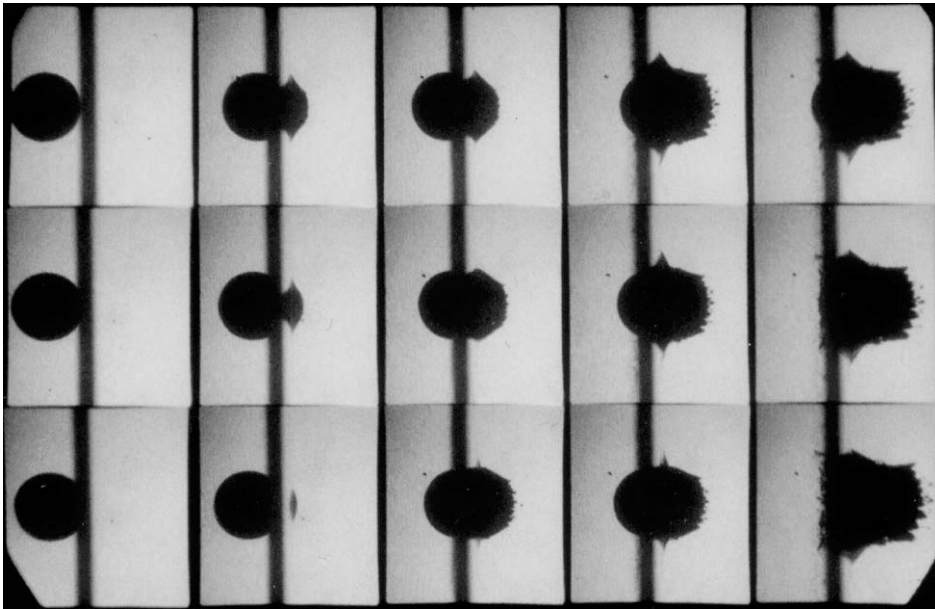


Fig. 5. An example record of 12.69 mm diameter spherical steel projectile impacting 3.21 mm thick PMMA at 465 m/s. Interframe time 1 μ s, exposure time 0.5 μ s.

the targets during the impact appeared to be restricted to a region of roughly the same size as the projectile; the remainder of the sample appeared to be unaffected. This observation confirms that the specimen dimensions (120 mm \times 120 mm) were large enough for reflections from the specimen edges to be ignored for the duration of the impact event. The present data, therefore, were effectively valid for “semi-infinite” plates. The records for each of the three different lay-ups were qualitatively similar. From streak records, Fig. 6, the velocity change during the impact can be determined, as can the velocity of ejected debris.

The front of the debris cloud ahead of the projectile was travelling almost three times faster than the projectile itself, as measured using Fig. 4. This cloud tends to obscure the out-of-plane deformation of the composite (Fig. 3). At lower velocities, near the ballistic limit, there would be less debris to obscure the plate deformation.

These measurements allow the kinetic energy lost by the projectile to be calculated (see Table 2). After impact, the unidirectional material showed significantly greater damage than the other composites. Figs. 7 and 8 show the macroscopic damage typically sustained by the three composite types. The PMMA absorbed the least energy per mm of thickness, and it fractured in a brittle fashion forming many angular fragments. Unlike CFRP, PMMA does not have any toughening mechanisms such as fibre pull-out and delamination.

The unidirectional samples showed extensive delamination along the fibres, which led to its macro-fragmentation. The other lay-ups show a roughly circular punched hole on the front face (Figs. 7(b) and 8(b)), with more serious damage exhibited on their rear faces (Figs. 7(a) and 8(a)). The shape of the penetration hole depended on the lay-up: rhombohedral in the case of type A and hexagonal in the case of type B composites. This agrees with previous work [12,13]. The

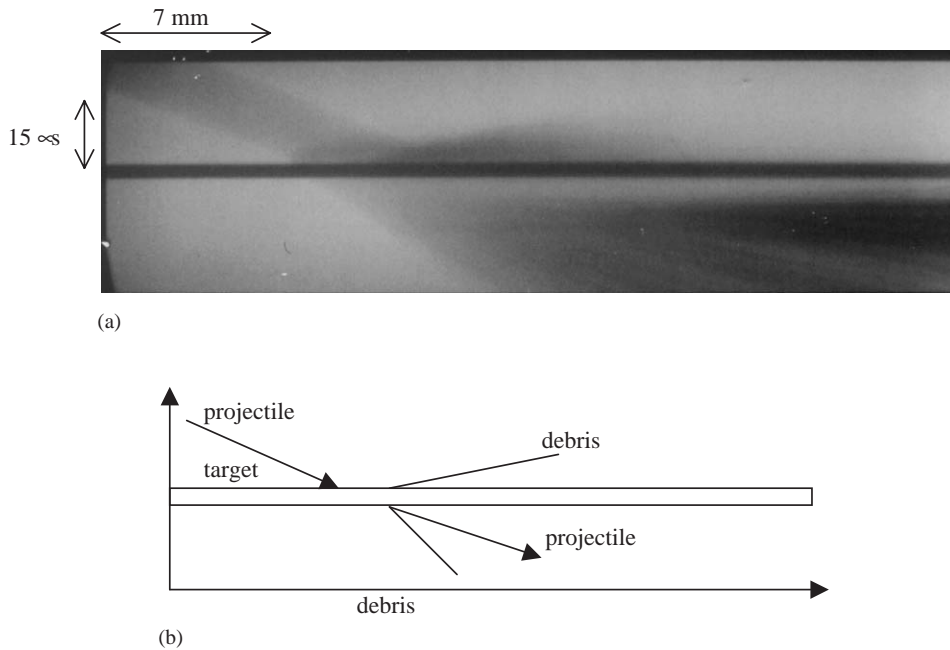


Fig. 6. (a) Streak record for 12.69 mm diameter steel projectile impacting a type B composite at 473 m/s. The horizontal line represents the sample, at the point of impact it can be seen that the projectile changes velocity (the diagonal band changes gradient). Streak speed $1.21 \pm 0.01 \mu\text{s}/\text{mm}$. (b) Schematic of the streak record.

Table 2
Comparison of energy absorbing properties of composites studied

Composite lay-up	Initial projectile velocity (m/s) ± 20	Residual projectile velocity (m/s) ± 20	Energy loss of projectile during impact (J) ± 20	Effective energy loss of projectile during impact (J/mm thickness) ± 20
A	477	240	720	320
B	473	210	730	290
C	472	250	690	390
PMMA	466	240	670	210

diameter of the hole increases through the thickness of the composite, and the perimeter of the hole is edged by protruding groups of fibres, indicating that fibre pull-out has occurred.

Figs. 7(a) and 8(a) also show extensive delamination of the outer ply on the rear of the target. In general, plies are constrained during the impact by those on either side, which are of different orientation. However, the rear ply is the most damaged in types A and B as it has no rear support. In a unidirectional composite, there is constraint only in one direction so cracking can easily travel between the plies (Fig. 9). The macroscopic damage in type B composites appears to be slightly greater than that seen in type A (Figs. 7 and 8). In order to interpret these results better, it is

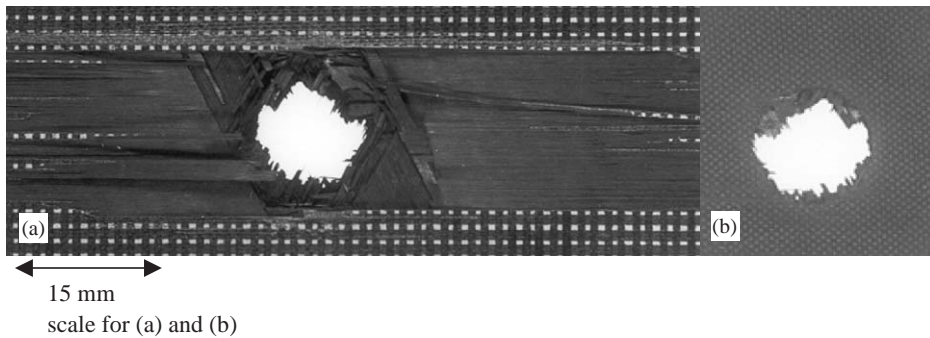


Fig. 7. Post-impact macroscopic damage to composite type A impacted at 460 m/s by 12.69 mm diameter steel sphere: (a) rear face of sample (grid pitch is 1.5 mm) and (b) front face of sample.

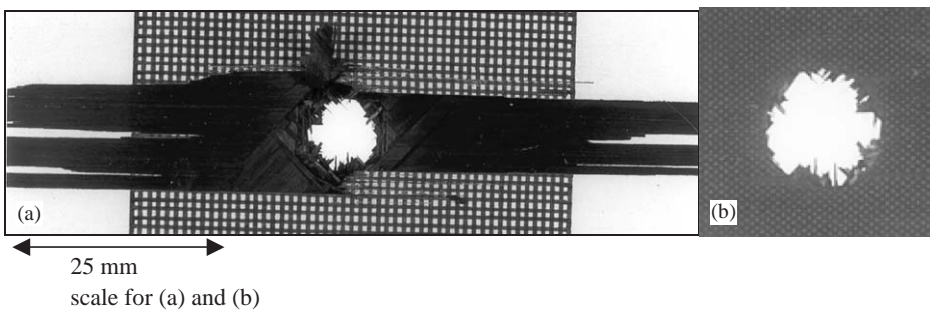


Fig. 8. Post-impact macroscopic damage to composite type B impacted at 460 m/s by 12.69 mm diameter steel sphere: (a) rear face of sample (grid pitch is 1.5 mm) and (b) front face of sample.

necessary to consider the microscopic deformation mechanisms in each lay-up. The average energy absorbed per unit thickness during impact is slightly lower for type B composite than type A (Table 2). In order to interpret these results better, it is necessary to consider the microscopic deformation mechanisms in each lay-up.

Dynamic impact damage in low toughness matrix laminates is usually characterised by a network of interlaminar and intralaminar cracks extending some distance beyond the impact zone [14]; see Figs. 10 and 11. These crack networks were observed and their extent measured using a travelling optical microscope. In type A composite, these crack networks penetrated to about 10 mm from the penetration hole, whereas in type B composites the crack networks extended through only 6 mm of the material. At the fracture face, fibre fragmentation is clear, as is fibre pull-out (Figs. 12 and 13).

Near the fracture, cracks propagate through the matrix within the plies (Fig. 10). These cracks terminate after a short distance (roughly 0.5 mm) unless they meet an interlaminar region. In the interlaminar regions, cracks propagate deep into the sample into a ply where a weakness such as a resin pocket exists (Fig. 14). This is seen in both A and B composites but over different length scales.

Throughout these samples there are pores of varying sizes, up to 1 mm in length, whose non-uniform distribution does not appear to depend upon the proximity of the fracture; pores seem to

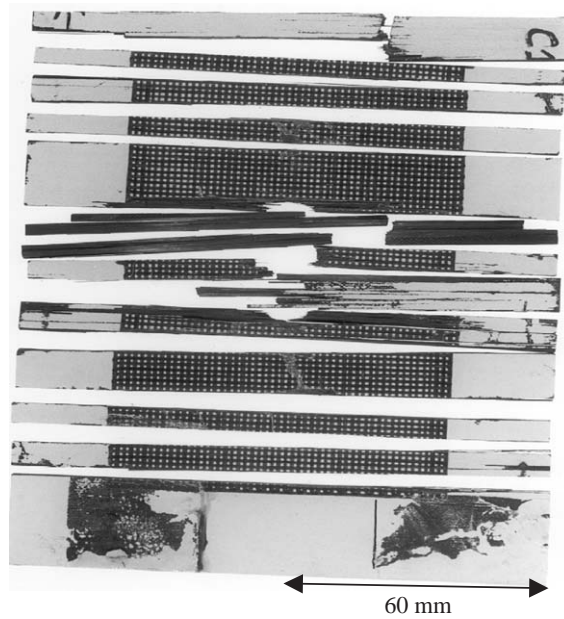


Fig. 9. Post-impact image of unidirectional composite impacted by a 12.69 mm diameter spherical steel projectile at 480 m/s. View of rear face.

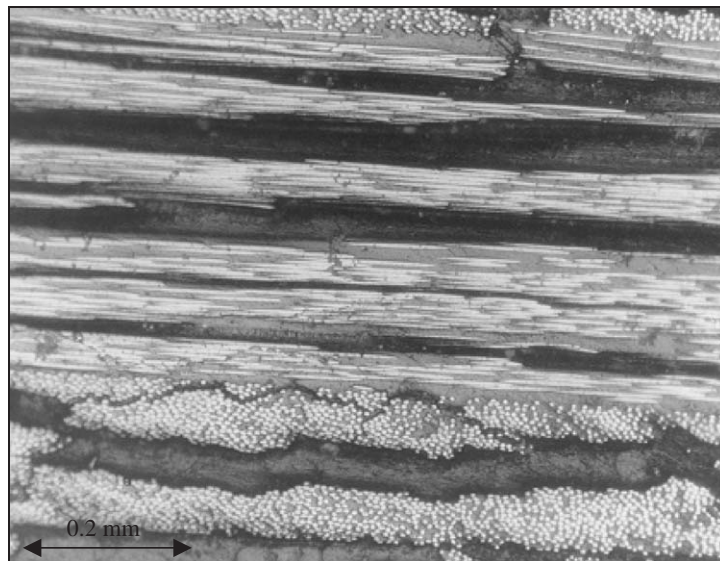


Fig. 10. Intralaminar cracking in type A composite.

be grouped together within single plies (Fig. 15). Their presence in unimpacted samples shows they are a feature of the composite manufacture process. There is some interaction between the crack network and these pores (Fig. 16), the presence of voids in laminates having a strong effect on both fracture toughness [13,15,16] and shear strength [17]. Because the distribution of void

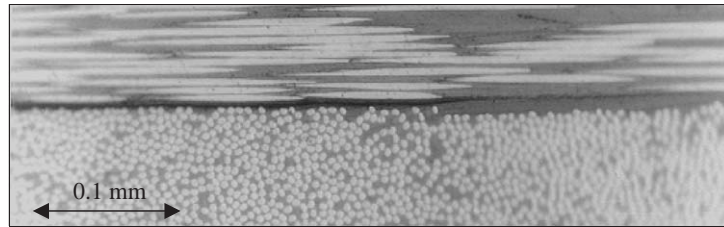


Fig. 11. Interlaminar crack termination on type A composite.

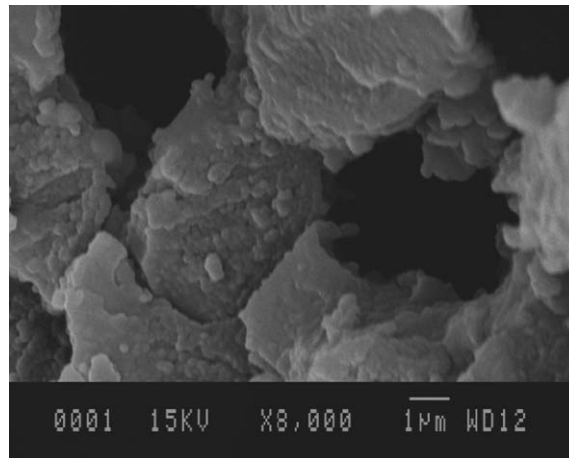


Fig. 12. SEM image showing holes which are evidence of fibre pull-out in type C composite.

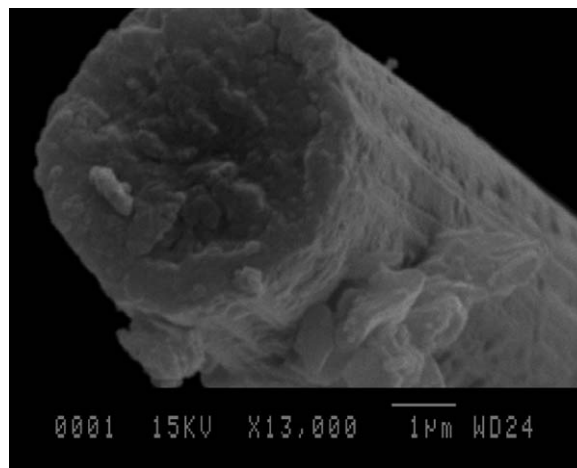


Fig. 13. SEM image showing relatively flat fracture face of pulled-out carbon fibre, with some matrix still present, for type A composite.

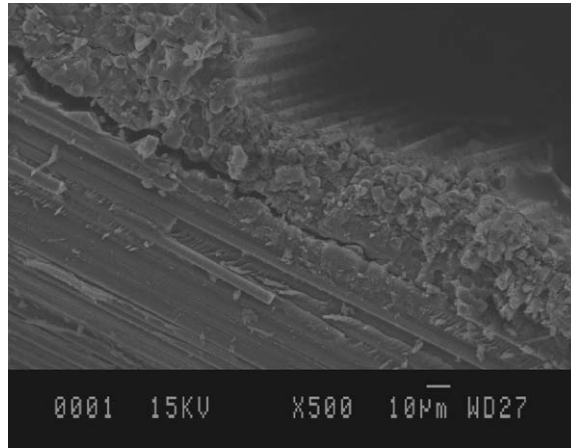


Fig. 14. SEM image showing intraply failure in type A composite.

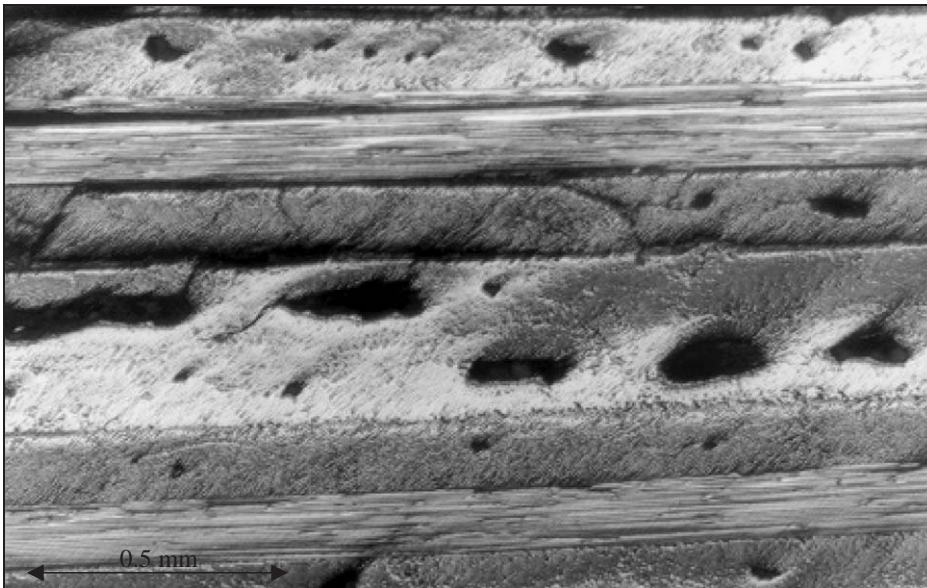


Fig. 15. Grouping of porosity in type B composite sample.

position and size is similar in each lay-up of composite the results of this work can be viewed as a valid comparison between different lay-ups. Even high-grade composites will probably display these features.

The fibre packing density can be assumed to be identical in each of the different lay-ups, therefore if the fibres fractured by the same mechanism the energy required would be identical and scale with the number of plies. Much of the remaining energy that is lost from the projectile during impact, is dissipated in growing both interlaminar and intralaminar cracks, and also in

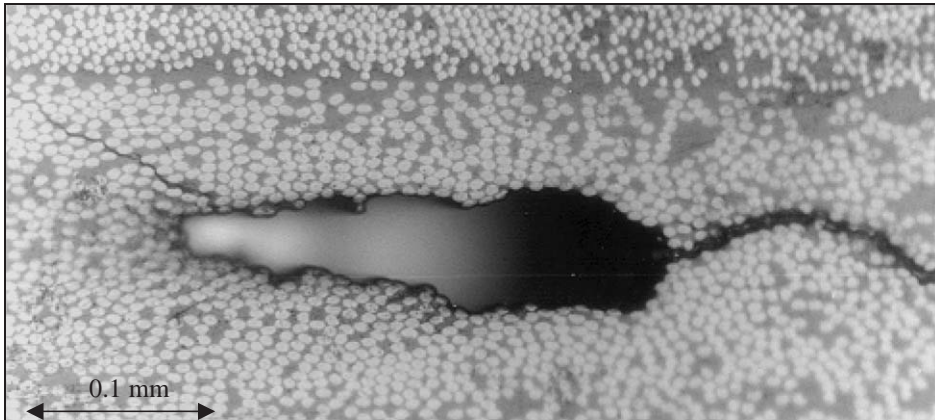


Fig. 16. Crack passing through a pore in type A composite sample.

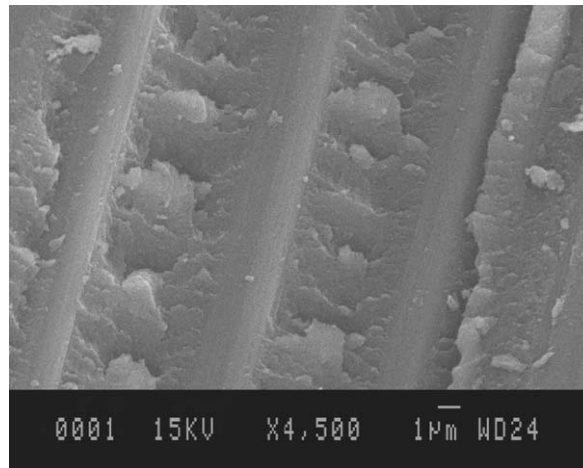


Fig. 17. SEM image showing matrix shear parallel to fibres in type B composite.

fibre pull-out and fracture. In type C composite, this is most effectively dissipated over the largest volume of material, which explains the higher energy loss of the projectile for this lay-up.

Examination of the fracture faces by SEM revealed that intralaminar failure parallel to fibres occurred by a mixture of localised matrix shear and matrix/fibre interfacial debonding (Figs. 17 and 18) in each of the composite lay-ups. A limited amount of interply delamination was also observed. The fracture face itself was relatively flat for the unidirectional material, probably due to the fact that plies were almost indistinguishable; in other lay-ups there were many distinct regions to the fracture face. The fibres showed very distinct fractures, all failures were initiated by cracks running perpendicular to the fibre axis. Some failure faces were relatively planar (Fig. 13) and others stepped (Fig. 19). All showed fractures characteristic of onion-skin structure carbon fibres [11]. Carbon fibres typically show very little ductility. All fracture faces examined exhibited brittle fracture.

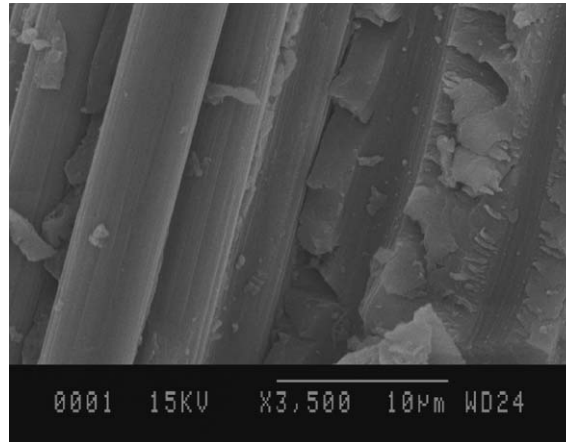


Fig. 18. SEM image showing fibre/matrix interfacial failure in type B composite.

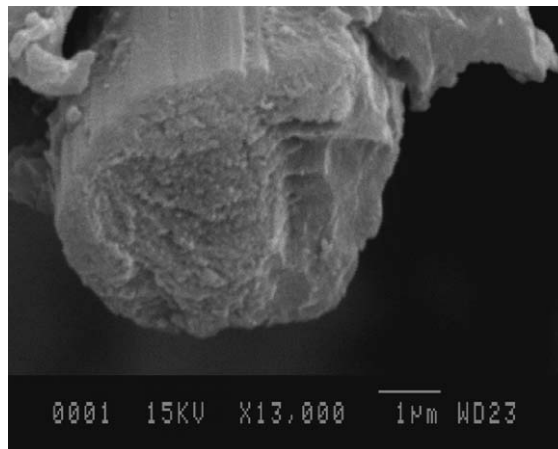


Fig. 19. SEM image showing stepped fracture face carbon fibre for type B composite.

Fig. 3 shows a typical record of a fine-grid shot. There was shadowing of the bulge and intense fragmentation at the rear producing a debris cloud obscuring a wide area of view after only a few frames in all instances. Therefore, fine-grid analysis was used only for the first few frames, after this there were a significant number of “cuts”, i.e. discontinuities, in the data. Using a second light source or a more complex array of mirrors, equal illumination of both sides of the bulge reduces this to some extent.

For the quasi-isotropic composite samples, the fine-grid results showed the majority of the material at the impact site moving in the positive x direction (Fig. 20(a) and (b)). This is probably due to the outer ply spalling off as a flap from the centre across the sample. This mode of failure is associated with reflection of the impact pulse at the rear surface. This also shows that the

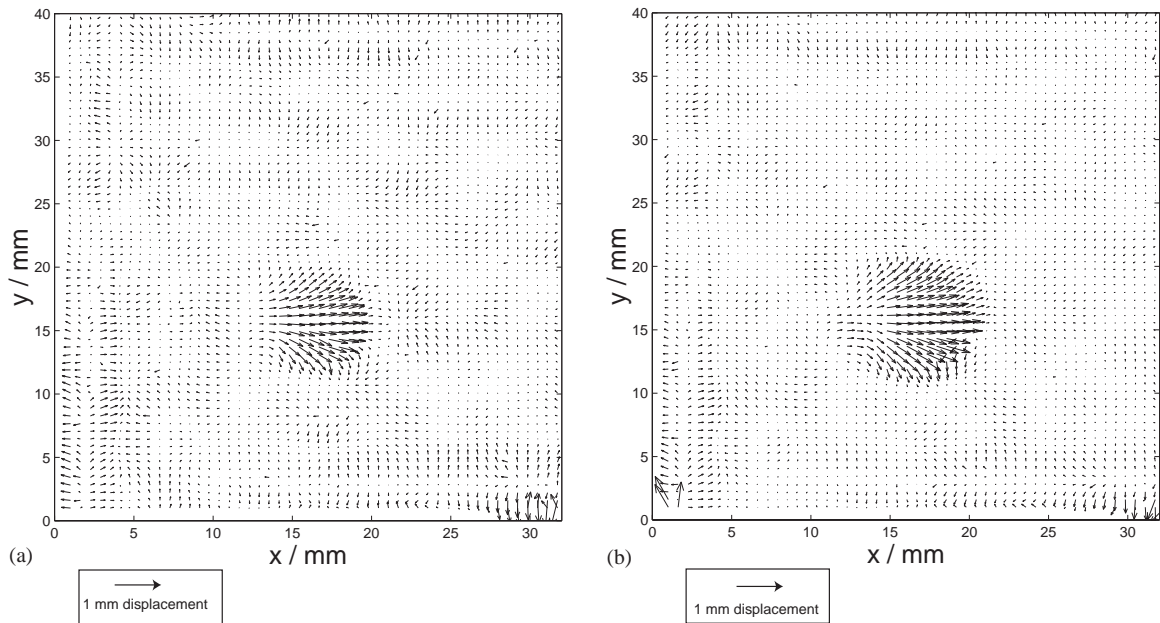


Fig. 20. In-plane displacement maps on the rear surface of a composite type B impacted by a 12.7 mm diameter steel sphere at 480 m/s. (a) 1.5 μ s and (b) 2.5 μ s after impact. Note the outer ply hinges outwards from the left-hand side along a vertical line at \sim 13 mm.

asymmetry of the rear face failure develops in the early stages (Figs. 7(a) and 8(a)). The magnitude of the noise in the data can be seen by looking at data points well away from the impact.

Fig. 20 shows the outer ply cracks perpendicular to the fibres (x -axis) on one side of the zone of material that was deformed by the impact. This may correspond to the extreme point of transverse disturbance in the fibre, which travels away from the impact at the speed of sound in the material. It seems quite likely that this fracture initiated at some discontinuity in the material such as a fibre flaw or pore. The behaviour of both composite types A and B were found to be similar. The unidirectional composite material exhibited deformation mainly in the x direction, perpendicular to the fibres (Figs. 21(a) and (b)). There are cracks generated parallel to the fibres in the centre of the impact region as seen in Fig. 21(a).

Fig. 22(a) shows that the deformation of PMMA is more isotropic than the composite 1 μ s after impact. Material moves away from the centre of impact in all directions and there is some evidence of radial cracking. For example, the line labelled C is indicative of radial crack growth. Later in the impact event the PMMA target fractures (Fig. 22(b)) and the fragments disperse in many directions, these fragments being indicated by blocks of parallel similarly sized displacement arrows.

In all cases, the deformation occurred over a region similar in area to the size of the projectile. This is clearly visible in Fig. 3, which covers a longer time period. This suggests that it was only during the latter part of penetration that matrix cracking propagated away from the impact site.

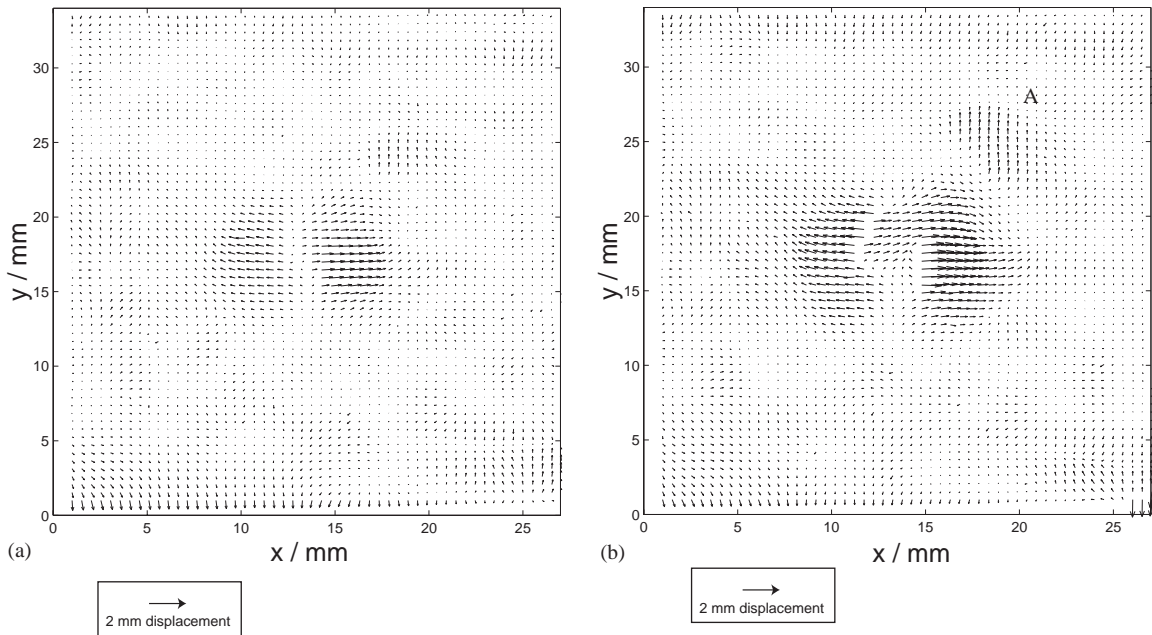


Fig. 21. In-plane displacement maps on the rear surface of composite type C, impacted by a 12.7 mm steel sphere at 450 m/s. (a) 2 μ s and (b) 3 μ s after impact. This is a unidirectional composite with the fibres aligned vertically. At 2 μ s, the surface is bulging outwards and there is failure along the central line. At 3 μ s, the bulge is cracking along a second failure line. It appears that delamination of the outer ply is occurring in the regions such as that labelled A.

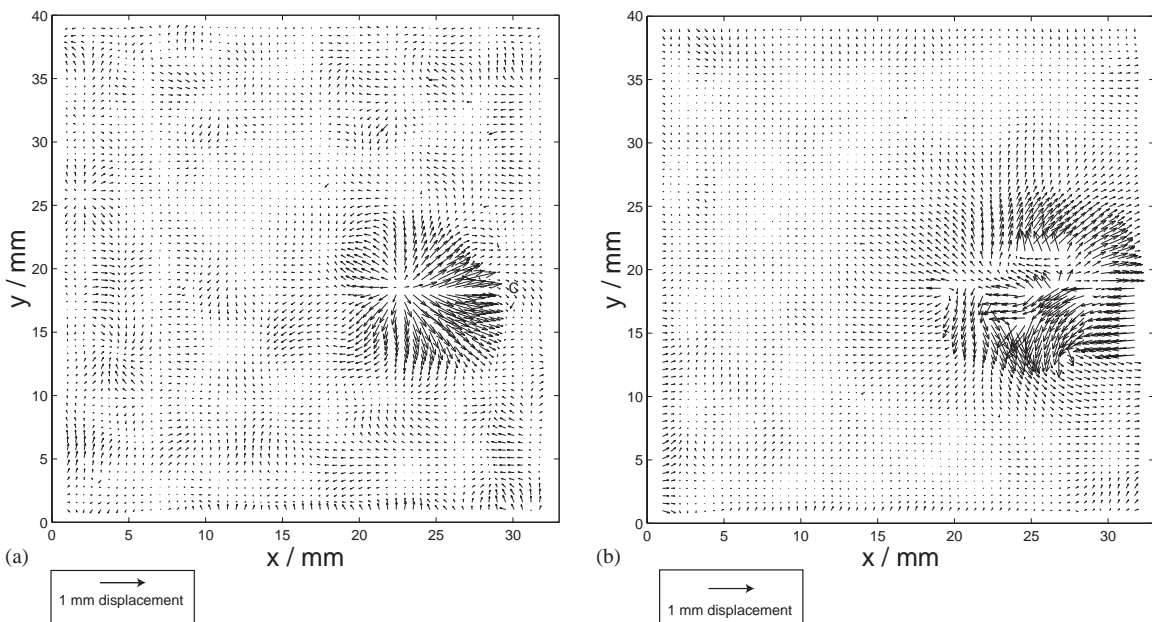


Fig. 22. In-plane displacement maps on the rear surface of PMMA, impacted by a 12.7 mm steel sphere at 480 m/s. (a) 1 μ s (b) 5 μ s after impact. PMMA is isotropic and at the 1 μ s stage the bulge is uniform though there is an indication of rear surface radial cracking. C marks the path of a radial crack. At 5 μ s, the brittle PMMA is intensely fractured.

4. Conclusions

Despite the fact that the macroscopic damage was very different for the unidirectional composite, the microstructural deformation mechanisms were found to be similar in all lay-ups, the major differences being the volume over which intense damage was spread.

Microstructural damage was characterised by a network of interlaminar and intralaminar cracks occurring by a mixture of matrix/fibre interfacial debonding and localised matrix shear. In all samples, the deformation observed, during the initial part of the impact, was restricted to an area the size of the projectile. However, post-impact damage was spread over an area of diameter of approximately three times (in the $[0^\circ/-45^\circ/45^\circ/90^\circ]_{2s}$ lay-up) to two times (in the $[0^\circ/60^\circ/-60^\circ]_{3s}$ lay-up) the diameter of the projectile. This may have been due to flexing after the initial penetration. Cracking occurred throughout the sample in both the unidirectional composite and the PMMA.

The fine-grid technique revealed that in the quasi-isotropic composite material the initial failure in the outer ply was due to cracks both perpendicular to and parallel to the fibres leading to delamination of the outer ply. The bulk material which was still visible outside this region of delamination did not appear to deform. The unidirectional composite material as expected exhibited the most anisotropic behaviour; deformation was mainly perpendicular to the fibre axis and cracks quickly formed parallel to the fibres, propagating rapidly across the whole sample. The deformation found in the PMMA sample was relatively isotropic until fragmentation.

In this impact velocity regime, where the outer ply detaches (spalls), the fine-grid technique results at late times have to be treated with caution. However, for early times or at velocities below the critical spall velocity, or with tougher composite systems it gives valuable quantitative information. In the present case, it establishes the origin of the failure process of the rear surface, the mode of deformation and the timescales involved. When two adjacent rows of arrows diverge, as in Fig. 22, this is indicative of radial crack growth.

In terms of energy dissipation during impact the $[0^\circ/-45^\circ/45^\circ/90^\circ]_{2s}$ lay-up performed slightly better than the $[0^\circ/60^\circ/-60^\circ]_{3s}$ lay-up. Both were substantially better at absorbing energy than the unidirectional material. This trend is reflected in the macroscopic damage; the lay-ups absorbing the least energy were the most damaged macroscopically and those dissipating the most energy appeared the least damaged. A probable reason for this is that the energy dissipated by propagating cracks, both interlaminar and intralaminar, through the material was spread over a larger volume in the $[0^\circ/-45^\circ/45^\circ/90^\circ]_{2s}$ lay-up than in the $[0^\circ/60^\circ/-60^\circ]_{3s}$ lay-up materials.

The unidirectional material allowed easy crack propagation across the whole sample as expected. Both microscopically and macroscopically the non-unidirectional composites behaved more isotropically than the unidirectional material.

Acknowledgements

The help received from Dr. P. Rae, R. Marrah and R. Flaxman at the Cavendish Laboratory and also D. Vowles of the Department of Materials Science and Metallurgy, Cambridge University was invaluable. We thank Professor V.B.C. Tan of the University of Singapore for providing samples.

References

- [1] Jacobs MJN, Van Dingenen JIJ. Ballistic protection mechanisms in personal armour. *J Mater Sci* 2001;36(13):3137–42.
- [2] Larsson F, Svensson L. Carbon, polyethylene and PBO hybrid fibre composites for structural lightweight armour. *Composites Part A-Applied Science and Engineering* 2002;33(2):221–31.
- [3] Navarro C. Simplified modelling of the ballistic behaviour of fabrics and fibre-reinforced polymeric matrix composites. *Key Eng Mat* 1998;141(1):383–99, Part 1–2.
- [4] Kelly A, editor. *Concise encyclopaedia of composite materials*, revised ed. Oxford: Pergamon Press, 1994.
- [5] Matthews FL, Rawlings RD. *Composite materials: engineering and science*, 1st ed. London: Chapman & Hall; 1994.
- [6] Harding J. In: Blazynski TZ, editor. *The effect of high strain rates on material properties*. Amsterdam: Elsevier, 1987. p. 133–86.
- [7] Rae PJ, Goldrein HT, Bourne NK, Proud WG, Forde LC, Liljekvist M. Measurement of dynamic large-strain deformation maps using an automated fine grid technique. *Opt Lasers Eng* 1999;31:113–22.
- [8] Goldrein HT, Palmer SJP, Huntley JM. Automated fine grid technique for measurement of large-strain deformation maps. *Opt Lasers Eng* 1995;23:305–18.
- [9] Bourne NK, Field JE. On the impact and penetration of transparent targets. *Proc R Soc Lond A* 1999;455: 4169–79.
- [10] Sun Q. *Solid particle erosion and ballistic impact*. PhD Thesis, Cambridge: Cavendish Laboratory and Cambridge University, 1991.
- [11] Day RJ. *Modelling of the micromechanics of the microbond test*. 2nd International Conference on Deformation and fracture of composites, UK, 1993. Institute of Materials, 1993.
- [12] Rogers KF, Sidey GR, Kingston-Lee DM. Ballistic impact resistance of carbon-fibre laminates. *Composites* 1971;2:237–41.
- [13] Gorham DA, Field JE. The failure of composite materials under high-velocity liquid impact. *J Phys D* 1976;9:1529–41.
- [14] Boll DJ, Bascom WD, Weidner JC, Murri WJ. A microscopy study of impact damage of epoxy-matrix carbon-fibre composites. *J Mater Sci* 1986;21:2667–77.
- [15] Putnam JW, Seferis JC, Pelton T. Influence of material characteristics on the fracture behaviour of polymeric composites. 2nd International Conference on Deformation and fracture of composites, UK, 1993. Institute of Materials, 1993.
- [16] Gorham DA, Matthewson MJ, Field JE. Damage mechanisms in polymers and composites under high-velocity liquid impact. In: Adler WF, editor. *Erosion: prevention and useful applications*. West Conshohocken, PA: ASTM; 1979. p. 320–42.
- [17] Gunyaev GM. The effect of structure processing defects on the mechanical properties of polymeric composites. In: Sih GC, Skudra AM, editors. *Failure mechanics of composites handbook of composites*. Amsterdam: Elsevier; 1985. p. 375–91.